ISSN 1001-0742
CN 11-2629/X

JES

JOURNAL OF ENVIRONMENTAL SCIENCES

March 1, 2015 Volume 29
www.jesc.ac.cn

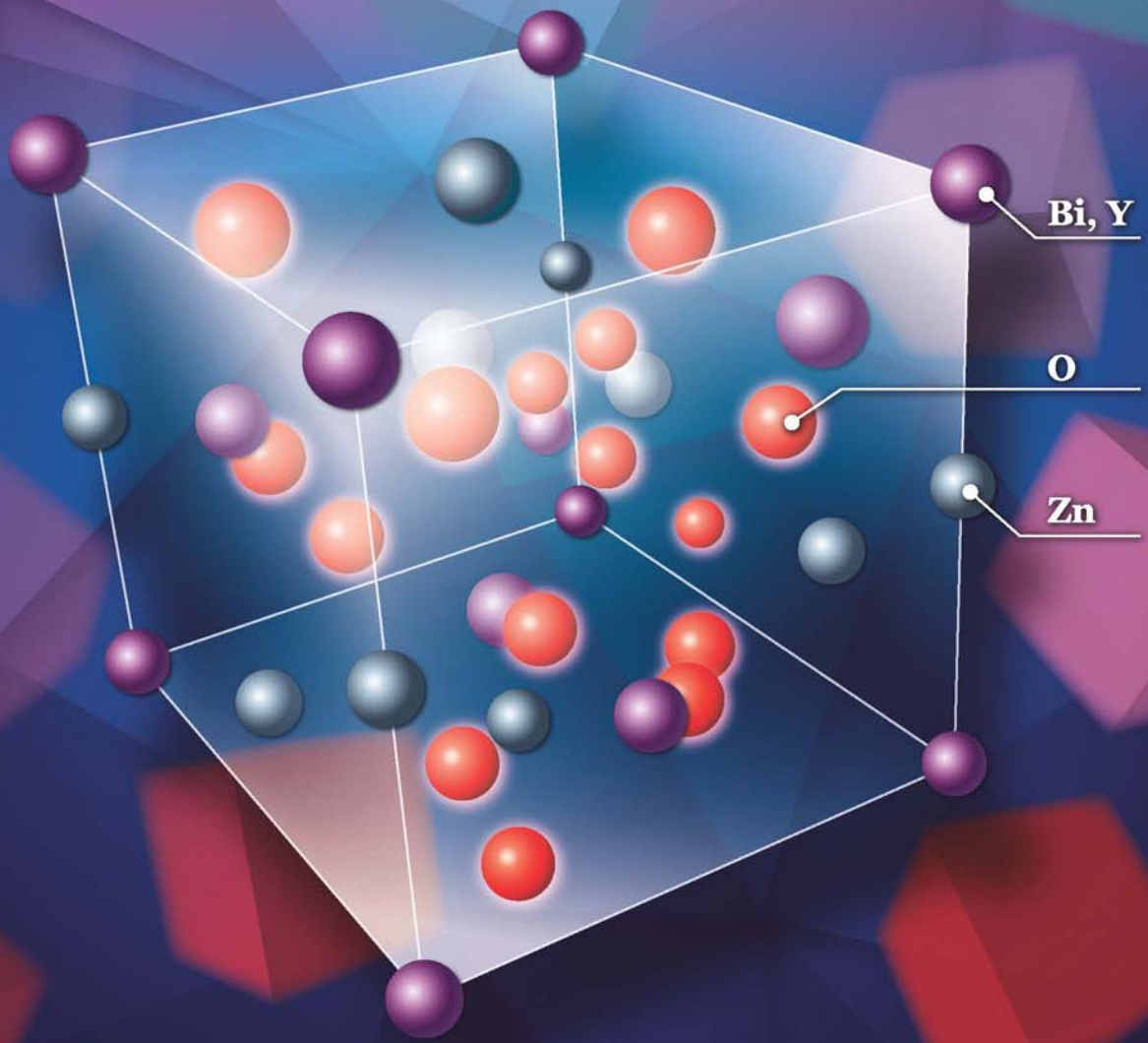

ELSEVIER
Science Press

Sponsored by
Research Center for Eco-Environmental Sciences
Chinese Academy of Sciences

Journal of Environmental Sciences Volume 29 2015

www.jesc.ac.cn

(continued on inside back cover)

CONTENTS

Available online at www.sciencedirect.com

ScienceDirect

www.journals.elsevier.com/journal-of-environmental-sciences

JOURNAL OF ENVIRONMENTAL SCIENCES
www.jesc.ac.cn

Phosphorus recovery from biogas fermentation liquid by Ca–Mg loaded biochar

Ci Fang[1], *Tao Zhang*[1,*], *Ping Li*[1], *Rongfeng Jiang*[1], *Shubiao Wu*[2], *Haiyu Nie*[3], *Yingcai Wang*[1]

1. *Key Laboratory of Plant–Soil Interactions of Ministry of Education, College of Resources and Environmental Sciences, China Agricultural University, Beijing 100193, China. E-mail: 948376144@qq.com*
2. *College of Engineering, China Agricultural University, Beijing 100083, China*
3. *College of Science, China Agricultural University, Beijing 100193, China*

ARTICLE INFO

Article history:
Received 19 April 2014
Revised 12 June 2014
Accepted 1 August 2014
Available online 7 January 2015

Keywords:
Phosphorus
Ca–Mg loaded biochar
Biogas fermentation liquid
Recovery

ABSTRACT

Shortage in phosphorus (P) resources and P wastewater pollution is considered as a serious problem worldwide. The application of modified biochar for P recovery from wastewater and reuse of recovered P as agricultural fertilizer is a preferred process. This work aims to develop a calcium and magnesium loaded biochar (Ca–Mg/biochar) application for P recovery from biogas fermentation liquid. The physico-chemical characterization, adsorption efficiency, adsorption selectivity, and postsorption availability of Ca-Mg/biochar were investigated. The synthesized Ca–Mg/biochar was rich in organic functional groups and in CaO and MgO nanoparticles. With the increase in synthesis temperature, the yield decreased, C content increased, H content decreased, N content remained the same basically, and BET surface area increased. The P adsorption of Ca–Mg/biochar could be accelerated by nano-CaO and nano-MgO particles and reached equilibrium after 360 min. The process was endothermic, spontaneous, and showed an increase in the disorder of the solid–liquid interface. Moreover, it could be fitted by the Freundlich model. The maximum P adsorption amounts were 294.22, 315.33, and 326.63 mg/g. The P adsorption selectivity of Ca–Mg/biochar could not be significantly influenced by the typical pH level of biogas fermentation liquid. The nano-CaO and nano-MgO particles of Ca–Mg/biochar could reduce the negative interaction effects of coexisting ions. The P releasing amounts of postsorption Ca–Mg/biochar were in the order of Ca–Mg/B600 > Ca–Mg/B450 > Ca–Mg/B300. Results revealed that postsorption Ca–Mg/biochar can continually release P and is more suitable for an acid environment.

Introduction

Phosphorus (P), as an essential element in the life process, may run out in several decade years (Gilbert, 2009). Meanwhile, a large number of P losses from the environmental processes (Elser and Bennett, 2011). In China, biogas fermentation liquid containing a large amount of P is the most important by-products of biogas engineering. The unreasonable treatment of biogas fermentation liquid may not only lead to P water eutrophication, but may also result in nonrenewable P resource (Loria et al., 2007). Hence, P recycling, that is, the recovery of P from biogas fermentation liquid and its reuse as fertilizer resource, is a new research focus.

Numerous P recovery technologies, such as chemical precipitation, biological P uptake, and adsorption, have been developed. However, chemical precipitation process may consume expensive chemicals and produce large amounts of chemical

* *Corresponding author*. E-mail: taozhang@cau.edu.cn (Tao Zhang).

http://dx.doi.org/10.1016/j.jes.2014.08.019

sludge (Zhang et al., 2014). Meanwhile, biological P uptake may be limited by the lack of carbon source and the difficult of culturing microorganisms (Rittmann et al., 2011). Carrying out adsorption has the advantages of easy controllability and low consumption (Yao et al., 2013). Recently, the application of biochar as an environment-friendly adsorbent has attracted attention, especially in P recovery studies.

Biochar made from agricultural waste corncob can be used for P recovery from agricultural wastewater biogas fermentation liquid. The P postsorption biochar can be reused as fertilizer for crop growth. Finally, crop wastes can be utilized to synthesize biochar. The easy controllability and low consumption of P adsorption can achieve environment and agriculture P recycling.

However, low efficiency and poor selectivity hamper the application of biochar adsorption for P recovery from wastewater. Hale et al. (2013) found that biochar only adsorbed 37.2% and 24.7% P. Yao et al. (2011b) demonstrated that the coexisting anions, Cl^-, NO_3^-, and HCO_3^- can decrease P adsorptive selectivity ratio by 4.3%, 11.7%, and 41.4%, respectively. To enhance P adsorption efficiency and selectivity, several researchers have developed new functional materials by loading cations, such as $La(OH)_3$-modified exfoliated vermiculites (Huang et al., 2014) and Fe-treated artificial zeolite (Johan et al., 2013).

The usability value of P postsorption biochar is important for its application of P reuse as agricultural fertilizer. Hale et al. (2013) indicated that the cacao-shell-made biochar can release 1484 ± 45 mg/kg of P after postsorption. However, the P available character of postsorption cation modified biochar has not been sufficiently studied.

In the present study, calcium and magnesium loaded biochar (Ca–Mg/biochar) was developed for P recycling. The Ca–Mg/biochar was synthesized at 300°C (Ca–Mg/B300), 450°C (Ca–Mg/B450), and 600°C (Ca–Mg/B600), and its characterization, adsorption efficiency, and selectivity were examined. The P availability of postsorption Ca–Mg/biochar was investigated.

1. Experiments

1.1. Materials

For the biochar sample, the ground corncob was initially dipped in $MgCl_2$ solution at a mass to volume ratio of 1:3 for 2 hr and then dried at 110°C. Afterwards, the dried Mg loaded corncob was dipped in $CaCl_2$ solution at a mass to volume ratio of 1:3 for 2 hr and then dried at 110°C. The Ca–Mg loaded corncob was respectively synthesized at 300°C, 450°C, and 600°C for 3 hr with nitrogen gas (limited oxygen), and then sieved into 0.1–0.2 mm. Finally, the synthesized Ca–Mg/biochar sample was cleaned with deionized water (DI) to removal residue surface ash. The Ca–Mg/biochar sample was dried and sealed in a container before use.

For the wastewater sample, the biogas fermentation liquid was extracted from a biogas fermenter in a pig farm near Beijing. The wastewater sample was centrifuged, filtered, and stored in an icebox prior to experiments. The component parameters are as following: pH 8.3, COD 850 mg/L. NH_4^+–N 620 mg/L, K^+ 253 mg/L, NO_3^-–N 215 mg/L, PO_4^{3-}–P 62 mg/L, and Cl^- 106 mg/L.

1.2. P recovery efficiency test of Ca–Mg/biochar

For the kinetic adsorption, 0.2 g Ca–Mg/biochar was mixed with 20 mL biogas fermentation liquid, and then shaken at 200 r/min at 303 ± 0.5 K. The supernatant was collected at a specific interval time.

For the adsorption isotherm, 0.2 g Ca–Mg/biochar was mixed with 20 mL P solution (diluted biogas fermentation liquid or mixed biogas fermentation liquid with NaH_2PO_4 to obtain the initial P concentration range of 30 to 4000 mg/L), and shaken at 200 r/min at 288 ± 0.5, 303 ± 0.5, and 318 ± 0.5 K for 12 hr until it achieved adsorption equilibrium.

1.3. P recovery selectivity test of Ca–Mg/biochar

For determination of the pH influence, 0.1 g Ca–Mg/biochar was mixed with 20 mL biogas fermentation liquid. The solution was adjusted at the given experimental pH of 4 to 10 and then shaken at 200 r/min at 303 ± 0.5 K for 12 hr.

To evaluate the influence of coexisting ions, 0.1 g Ca–Mg/biochar was mixed with 20 mL biogas fermentation liquid and P synthesis solution (DI mixed with NaH_2PO_4 at 62 mg/L P concentration) at pH = 9, and then shaken at 200 r/min at 303 ± 0.5 K for 12 hr.

1.4. P available test of postsorption Ca–Mg/biochar

For the continuous extraction, 0.1 g postsorption Ca–Mg/biochar (0.1 g Ca–Mg/biochar mixed with 2000 mL biogas fermentation liquid at 303 ± 0.5 K for 12 hr) was mixed with 120 mL DI or DI with 2% citric acid (citric acid DI), and then shaken at 200 r/min at 303 ± 0.5 K. The supernatant was collected at a specific reaction time.

For the interval extraction, after continuous extraction, 0.1 g postsorption Ca–Mg/biochar was mixed with 120 mL DI or citric acid DI and then shaken at 200 r/min at 303 ± 0.5 K. The supernatant was replaced with fresh extraction solution every 24 hr. The interval extraction was repeated six times.

1.5. Analysis

Ca–Mg/B300, Ca–Mg/B450, Ca–Mg/B600, and ground corncob were analyzed by CHN element analyzer (vario EL, Hanau, Germany), BET Surface Area Analyzer (BET, ASAP 2020, Atlanta, Georgia, USA), Fourier Transform Infrared Spectrometer (FT-IR, Magna-IR 750, Washington, USA), and Transmission Electron Microscope with Energy Dispersive X-ray spectrometer (TEM-EDX, JEM-2100F, Tokyo, Japan).

The collected supernatants were quickly filtered and measured. The PO_4^{3-}–P concentrations of supernatant were measured according to standard methods (APHA, 2012, 4500-P C. vanadomolybdophosphoric acid colorimetric method). All the experiments were repeated three times and the average values were calculated.

2. Results and discussion

2.1. Characterization analysis

Yield analysis (Table 1) showed the yield weight of Ca–Mg/biochar decreased from 58.09% to 36.97% with increasing synthesis temperature. The analysis of CHN elements showed that with increasing synthesis temperature, C content

Table 1 – Characteristic of Ca–Mg/biochar and ground corncob.

Analysis items	Ca–Mg/B300	Ca–Mg/B450	Ca–Mg/B600	Ground corncob
Yields (wt.% wet basis)	58.09	40.20	36.97	
Elemental (wt.% dry basis)				
C	43.29	57.27	60.97	35.46
H	5.00	3.19	2.19	6.33
N	0.62	0.66	0.63	0.72
BET-N_2 surface area (m^2/g dry basis)	377.98	418.72	487.49	

increased from 43.29% to 60.97%, H content decreased from 5.00% to 2.19%, and N content was obviously unchanged. The change in C and H content of Ca–Mg/biochar demonstrated chemical bond fractures and material composition changes (Demirbas, 2004). N content remained unchanged because no nitrogenous volatile materials were formed (Gaskin et al., 2008). In general, the thermal decomposition of hemicellulose, cellulose, and lignin, as the main components of corncob, occurred in the temperature range of 190–320°C, 280–400°C, and 320–450°C, respectively (Strezov et al., 2012). The flammable compositions of corncob, such as cellulose, hemicelluloses, and lignin, were destroyed and volatilized with increasing synthesis temperature (Al-Wabel et al., 2013).

BET surface area analysis (Table 1) showed that the BET surface area of Ca–Mg/biochar increased with increasing synthesis temperature. The carbon structure of Ca–Mg/biochar was varied according to different synthesis pyrogenation processes, and numerous mesopores were generated in Ca–Mg/biochar. About 50% amylum and 30%–40% cellulose content of ground corncob were decomposed and generated carbon structure mesopores when pyrogenation temperature was lower than 500°C, or resulted in carbon structure collapse when pyrogenation temperature was increased to 600°C (Tang et al., 2013).

FT-IR analysis (Fig. 1a) detected the chemical bond structure of organic components for Ca–Mg/biochar and corncob. With increasing synthesis temperature, the characteristic peaks at 3274 cm^{-1}, 2936 cm^{-1}, 2896 cm^{-1}, and 1000–1400 cm^{-1} of ground corncob disappeared. The O–H, N–H, methyl (–CH_3), and ethyl (CH_2) were extremely unstable and ruptured with ease at high temperature level. The characteristic peaks at 3420 cm^{-1}, 1630 cm^{-1}, 1420 cm^{-1}, 800–900 cm^{-1}, and 500–800 cm^{-1} of Ca–Mg/biochar were stable and were enhanced with increasing synthesis temperature (Hossain et al., 2011). The presence of C═O, C═C (Chen et al., 2008), –COOH, CH_3O–, and Mg–O and O–Mg–O (Zhang et al., 2013) were formed in Ca–Mg/biochar. The characteristic peaks at 3420 cm^{-1} deepened with increasing synthesis temperature which indicated that more C═O and C═C were formed. Novak et al. (2009) reported that poly-condensed aromatic C-type compounds can be formed in biochar when the synthesis temperature is above 400°C. The results of FT-IR analysis in the present study indicated that the synthesized Ca–Mg/biochar was rich in organic functional groups of hydroxyl, carboxyl, carbonyl, and methoxyl, which were helpful for adsorption (Geng et al., 2009).

TEM analysis (Fig. 1b–d) showed that with increasing synthesis temperature of Ca–Mg/biochar, the number of mesoporous structures increased and the distribution of mesoporous structures turned from ordered to disordered. The number and distribution of mesopores are important factors for Ca–Mg/biochar adsorption. A considerable number of nanoparticles were present in the mesoporous structures of Ca–Mg/biochar. The characteristic peaks of Mg and Ca in EDX

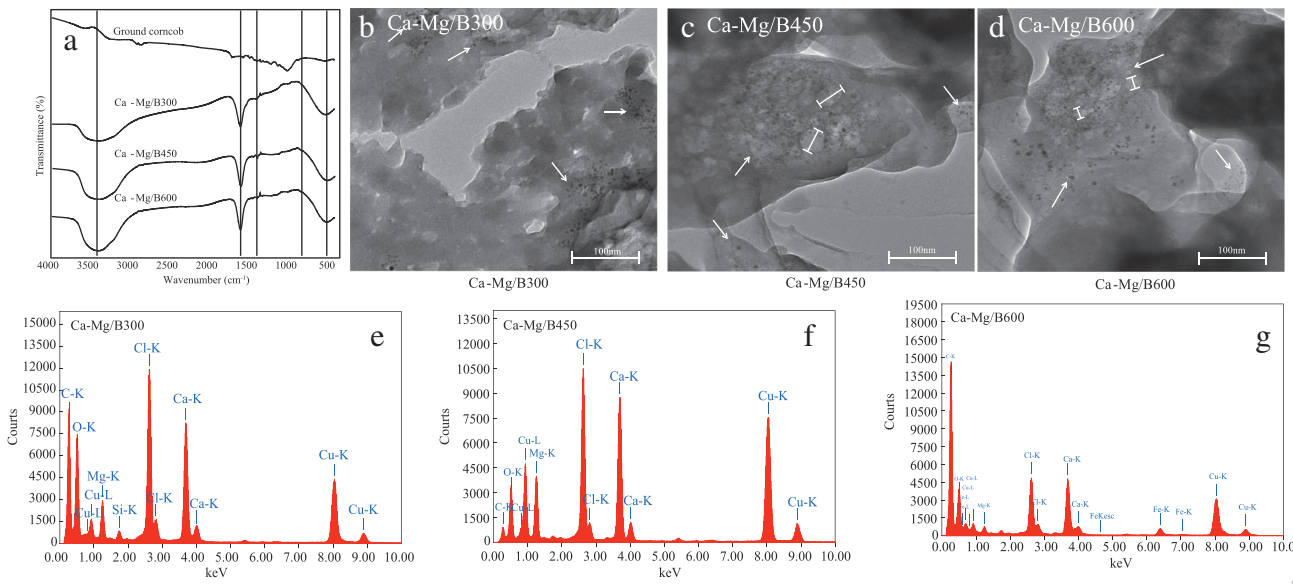

Fig. 1 – FT-IR analysis (a), TEM analysis (b–d), and EDX analysis (e–g) of Ca–Mg/biochar.

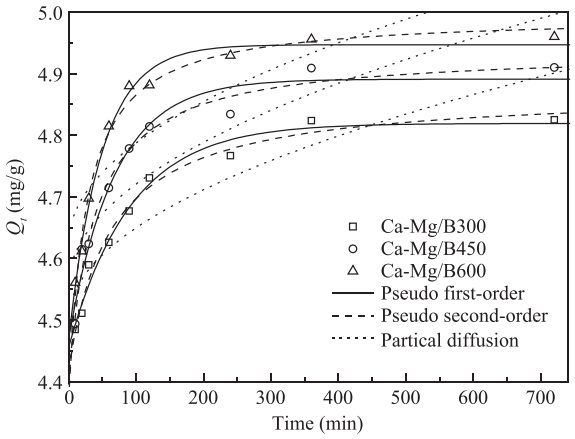

Fig. 2 – P adsorption kinetic analysis of Ca–Mg/biochar. (Q_t represents the P adsorbed amount at adsorption time t)

analysis (Fig. 1e–g) demonstrated that the observed nanoparticles were nano-MgO and nano-CaO particles.

The mesoporous structure was slightly opened for Ca–Mg/B300, and the adsorption effect mainly relied on the chemical actions of nano-MgO and nano-CaO particles. For Ca–Mg/B450, many mesoporous structures were opened (around 30–40 nm). The adsorption effect relied on Ca–Mg chemical actions and a certain extent of physical adsorption. For Ca–Mg/B600, the mesoporous structure was completely opened and even collapsed with the size of approximately 15–25 nm, which further resulted in an increase in surface area. The adsorption effect strongly relied on physical adsorption and chemical reaction (Chen et al., 2011).

2.2. P recovery efficiency of Ca–Mg/biochar

2.2.1. Adsorption kinetics

P adsorption kinetics of Ca–Mg/biochar (Fig. 2) indicated that the P adsorption equilibriums of Ca–Mg/B300, Ca–Mg/B450, and Ca–Mg/B600 were reached after 360 min. The adsorption rate of Ca–Mg/biochar was faster than that of other kinds of biochar reported in previous publications. Yao et al. (2011b, 2013) synthesized biochar through anaerobic digested sugar beet tailings, and tomato leaves, respectively and obtained the P adsorption equilibrium after 24 hr. Therefore, the presence of nano-CaO and nano-MgO particles in biochar can accelerate P adsorption rate. Due to its ability to reach adsorption equilibrium faster, the Ca–Mg/biochar is more suitable for use as filter material in fluidized beds compared with other types of biochar (Zhang et al., 2013).

Three kinetic models including pseudo first-order (Eq. (1)), pseudo second-order (Eq. (2)) and particle diffusion equation (Eq. (3)) were used to fit the P adsorption kinetics of Ca–Mg/biochar.

$$\ln(Q_e - Q_t) = \ln Q_e - k_1 t \quad (1)$$

$$\frac{t}{Q_t} = \frac{1}{k_2 Q_e^{\,2}} + \frac{t}{Q_e} \quad (2)$$

$$Q_t = k_{id} t^{\frac{1}{2}} + C \quad (3)$$

where, Q_e (mg/g) represents the P adsorbed amount at adsorption equilibrium; Q_t (mg/g) represents the P adsorbed amount at adsorption time t; k_1 (min^{-1}), k_2 (g/(mg·min)); and k_{id} (g/(mg·min)) represent the reaction rate constants; and C is a constant related to boundary layer thickness. Table 2 shows the P adsorption kinetic parameters of Ca–Mg/biochar.

The P adsorption of Ca–Mg/B300 and Ca–Mg/B450 was confirmed to the pseudo second-order kinetic and indicated that P adsorption was mainly controlled by chemical actions. The chemical combination of nano-CaO and nano-MgO particles with P was the major reaction rate control step for P adsorption. The P adsorption of Ca–Mg/B600 was confirmed to the pseudo first-order kinetic and indicated that the P adsorption reaction rate was mainly controlled by physical actions. k_1 and k_2 represent the P adsorption power of Ca–Mg/biochar. The k_2 of Ca–Mg/B300 and Ca–Mg/B450 were 0.00328 and 0.00529 (g/(mg·min)), respectively, which were six to ten times faster than that of biochar made from tomato leaves (0.000533 g/(mg·min)) (Yao et al., 2013). k_1 of Ca–Mg/B600 was 0.02034 min^{-1}, which was 7.85 times faster than that of biochar made from anaerobic digested sugar beet tailings (0.00259 min^{-1}) (Yao et al., 2011b). Therefore, Ca–Mg/biochar quickly reached P adsorption equilibrium. The particle diffusion fitting equation of Ca–Mg/biochar did not pass through the origin, which indicated that the P adsorption process was also influenced by particle internal diffusion action (Venkata Mohan et al., 2002).

Table 2 – P adsorption kinetic parameters of Ca–Mg/biochar.

Sample	Pseudo first-order			Pseudo second-order			Piratical diffusion		
	k_1	Q_e	R^2	k_2	Q_e	R^2	k_{id}	C	R^2
Ca–Mg/B300	0.01090	4.8194	0.9756	0.00328	4.8715	0.9795	0.01494	4.5002	0.8086
Ca–Mg/B450	0.01455	4.8912	0.9567	0.00529	4.9376	0.9756	0.01636	4.5572	0.7549
Ca–Mg/B600	0.02034	4.9471	0.9883	0.00765	4.9948	0.9842	0.01628	4.6245	0.6557

Note: k_1 represents reaction rate constant of pseudo first-order adsorption kinetic model. Q_e represents the P adsorbed amount at adsorption equilibrium. R^2 represents relevant coefficient. k_2 represents reaction rate constant of pseudo second-order adsorption kinetic model. k_{id} represents reaction rate constant of piratical diffusion adsorption kinetic model. C is a constant relate to boundary layer thickness.

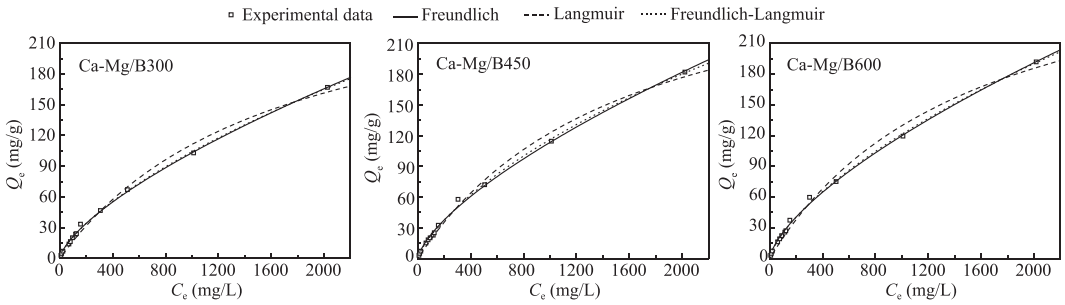

Fig. 3 – P adsorption isotherm analysis of Ca–Mg/biochar. (Q_e represents the P adsorbed amount at adsorption equilibrium)

2.2.2. Adsorption isotherms

The P adsorption isotherm of Ca–Mg/biochar (Fig. 3) is described by three kinds of isotherm equations.

The Freundlich adsorption isothermal equation describes the non-ideal adsorption on non-uniform surface, which can be expressed as follows:

$$Q_e = K_F C_e^{1/n}. \quad (4)$$

Langmuir adsorption isothermal equation describes the monolayer adsorption on uniform surface, which can be expressed as follows:

$$Q_e = \frac{Q_m K_L C_e}{1 + K_L C_e}. \quad (5)$$

The Langmuir–Freundlich adsorption isothermal equation describes the integrated empirical adsorption isothermal equations of Freundlich and Langmuir. The equation can be expressed as follows:

$$Q_e = \frac{Q_m K C_e^{1/n}}{1 + K C_e^{1/n}} \quad (6)$$

where, K_F ((L/g)$^{1/n}$), K_L (L/g), and K (L/g) represent the constants of the Freundlich, Langmuir, and Langmuir–Freundlich adsorption isothermal equations, respectively; $1/n$ is a parameter relevant to the reaction strength between adsorbed molecules and adsorbent surface; and Q_m (mg/g) denotes monolayer adsorption capacity.

The Freundlich model and Langmuir–Freundlich model matched the experimental data better ($R^2 > 0.99$) than the Langmuir model (Table 3). It indicated that Freundlich adsorption model was the main adsorption type. In the Freundlich model, $1/n$ value represents the heterogeneity of the site energies, which were divided into five levels (Tseng and Wu, 2008). With decreasing $1/n$ value, the adsorption became more favorable. The $1/n$ values of Ca–Mg/biochar for P adsorption were between 0.6 and 0.8 and belong to pseudo-linear level adsorption. With increasing synthesis temperature, the $1/n$ values of Ca–Mg/biochar decreased and further resulted in P adsorption tended to be favorable adsorption. Ca–Mg/biochar can highly absorb P with increasing synthesis temperature even at low concentration level (Tseng and Wu, 2008). K_F is the constant related to adsorption capacity. With increasing synthesis temperature, the K_F value of Ca–Mg/biochar increased, which indicated that P adsorption capacity increased (Oztürk and Bektaş, 2004). The maximum P adsorption amounts of Ca–Mg/B300, Ca–Mg/B450, and Ca–Mg/B600, obtained from the Langmuir adsorption isothermal model were up to 294.22, 315.33, and 326.63 mg/g, respectively. The results were consistent with the K_F value calculation and higher than those of former studies (Hale et al., 2013; Yao et al., 2011a). Moreover, the increase in K_L value further demonstrated that the P adsorption ability of Ca–Mg/biochar increased with increasing synthesis temperature. K_L is also related to adsorption strength. With increasing K_L value, the adsorption ability of Ca–Mg/biochar for low P concentration solution increased. Considering that the R^2 values of the three models were quite similar, the P adsorption of Ca–Mg/biochar was considered to be controlled by multiple processes. The results obtained were consistent with the results of previous research (Yao et al., 2013).

Table 3 – P adsorption isotherms parameter of Ca–Mg/biochar.

Sample	Freundlich			Langmuir			Langmuir–Freundlich		
	K_F	$1/n$	R^2	K_L	Q_m	R^2	K	$1/n$	R^2
Ca–Mg/B300	0.9129	0.6843	0.9985	0.6084	294.2177	0.9903	0.4311	0.7162	0.9984
Ca–Mg/B450	1.0214	0.6818	0.9970	0.6373	315.3268	0.9921	0.8044	0.7599	0.9976
Ca–Mg/B600	1.1483	0.6729	0.9977	0.6586	326.6284	0.9892	0.5356	0.7113	0.9976

Note: k_F represents reaction rate constant of Freundlich isotherm model. n is a parameter relevant to the reaction strength between adsorbed molecules and adsorbent surface. R^2 represents relevant coefficient. k_L represents reaction rate constant of Langmuir isotherm model. Q_m denotes monolayer adsorption capacity. K represents reaction rate constant of Langmuir-Freundlich isotherm model.

2.2.3. Thermodynamic calculation

The P adsorption thermodynamic calculation for Ca–Mg/biochar at 288, 303, and 318 K was analyzed. The Freundlich model was used to calculate the differential enthalpy of adsorption (ΔH), adsorption free energy (ΔG), and adsorption entropy (ΔS). The P adsorption of Ca–Mg/biochar was endothermic, spontaneous, and showed an increase in disorder of the solid–liquid interface.

Adsorption enthalpy is closely related to adsorption amount. When the adsorption amount is initialized at one value, the corresponding adsorption enthalpy is called the differential enthalpy of adsorption. The calculation formula can be expressed as follows:

$$\ln\left(\frac{1}{C_e}\right) = \ln K' - \frac{\Delta H}{RT} \tag{7}$$

where, R (8.314 J/(mol·K)) represents the ideal gas constant, T (K) represents the thermodynamic temperature, and K' represents a constant.

Adsorption free energy (ΔG) can be calculated through the Gibbs equation, which can be expressed as follows:

$$\Delta G = -RT\int_0^x \left(\frac{q'}{x}\right)dx \tag{8}$$

where, x represents the mole fraction of solute in the solution, and q' (mmol/g) represents the adsorption amount of adsorbent. Given that ΔG is irrelevant to q', the formula can be expressed as follows:

$$\Delta G = -nRT. \tag{9}$$

Adsorption entropy (ΔS) can be calculated by ΔH and ΔG. The formula can be expressed as follows:

$$\Delta S = \frac{(\Delta H - \Delta G)}{T}. \tag{10}$$

Table 4 shows the thermodynamically calculated ΔH, ΔG, ΔS of Ca–Mg/biochar. The ΔH values of Ca–Mg/B300, Ca–Mg/B450, and Ca–Mg/B600 were positive values, which indicated that the adsorption was an endothermic reaction. The ΔG values of Ca–Mg/B300, Ca–Mg/B450, and Ca–Mg/B600 were less than 0, indicating that P spontaneously tends to move from the solution to the Ca–Mg/biochar surface. With increasing adsorption reaction temperature, the ΔG values decreased, which indicated a better P adsorption efficiency of Ca–Mg/biochar at a higher solution temperature (Chen and Lu, 2014). The ΔS values of Ca–Mg/B300, Ca–Mg/B450, and Ca–Mg/B600 were positive values, which indicated that the disorder of the solid–liquid interface increased during adsorption and P tended to be adsorbed on the surface of Ca–Mg/biochar. This result may be attributed to the reaction of P to the nano-MgO and nano-CaO particles at the activity adsorption site (Unlu and Ersoz, 2006). Furthermore, ΔS decreased with increasing adsorption reaction temperature. In general, adsorption and desorption occur simultaneously. The increase or decrease of ΔS depends on the effect of desorption and adsorption. Therefore, the decrease in value means the ΔS decrease of adsorption became much more powerful than the ΔS increase of desorption at a higher reaction temperature. Yoon et al. (2014) and Tu and You (2014) found similar results during P adsorption on magnetic iron oxide nanoparticles and green synthesized nano-bimetal ferrites, respectively.

Table 4 – P adsorption thermodynamics calculation parameter of Ca–Mg/biochar.

Sample	Temperature (K)	ΔH (kJ/mol)	ΔS (J/(mol·K))	ΔG (kJ/mol)
Ca–Mg/B300	288	1.452	10.481	−1.662
	303		10.461	−1.724
	318		10.387	−1.747
Ca–Mg/B450	288	1.319	10.814	−1.656
	303		10.334	−1.718
	318		9.859	−1.773
Ca–Mg/B600	288	1.228	10.147	−1.611
	303		9.727	−1.695
	318		9.368	−1.751

2.3. P recovery selectivity of Ca–Mg/biochar

2.3.1. pH influence

The resistant ability of the solution pH is an important indicator to evaluate P recovery selectivity of Ca–Mg/biochar. As shown in Fig. 4 the pH resistant ability of Ca–Mg/B600 for P adsorption was not influenced by solution pH. While, for Ca–Mg/B450 and Ca–Mg/B300, owing to the presence of nano-CaO and nano-MgO particles, the optimal solution pH range for P selectivity adsorption was 8 to 9, which was close to the pH range of raw biogas fermentation liquid. Therefore, the P adsorption selectivity of Ca–Mg/biochar cannot be significantly influenced by the typical pH value of biogas fermentation liquid.

Considering the ionization constants of phosphoric acid ($pKa_1 = 2.15$, $pKa_2 = 7.20$, $pKa_3 = 12.33$), P was present in different superior forms depending on pH. When pH

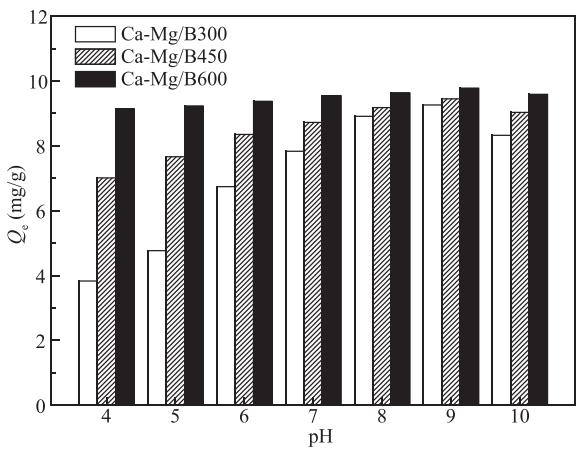

Fig. 4 – pH influence on P adsorption selectivity of Ca–Mg/biochar. (Q_e represents the P adsorbed amount at adsorption equilibrium)

increased from 4 to 7, $H_2PO_4^-$ was the superior form in the solution, while HPO_4^{2-} was the superior form in the solution when pH increased from 7 to 10. The $H_2PO_4^-$ form was unfavorable for the reaction of CaO and MgO with P. The nanoparticles of CaO and MgO could capture the HPO_4^{2-} form with ease (Chen et al., 2007).

The adsorption effect of Ca–Mg/B300 mainly relied on the nanoparticles of CaO and MgO, and the resistant ability of the solution pH was weak. When pH changed from 4 to 5, the presence of CaO and MgO nanoparticles in biochar did not react with P efficiency. The impact of physical adsorption was weak, and P adsorption ability was relatively low. When pH increased from 6 to 9, the nanoparticles of CaO and MgO enhanced P adsorption effect (Wajima and Rakovan, 2013) and reached the maximum amount at pH 9.0. When pH reached 10, OH^- in solution could compete with P (Yao et al., 2011b) and react with the nanoparticles of CaO and MgO.

The adsorption effect of Ca–Mg/B450 relied on the chemical reaction of CaO and MgO nanoparticles and the physical adsorption of mesopore structure. The resistant ability of the solution pH of Ca–Mg/B450 was better than that of Ca–Mg/B300. When pH increased from 4 to 5, Ca–Mg/B450 mainly relied on physical adsorption. Chemical adsorption gradually increased with increasing pH and achieved the maximum amount at pH 9. Therefore, adsorption selectivity could be enhanced by the CaO and MgO nanoparticles. When pH reached 10, P adsorption amount slightly decreased because of the competition with OH^-.

The adsorption effect of Ca–Mg/B600 mainly relied on a stronger physical adsorption and the reaction of CaO and MgO nanoparticles. The solution pH did not have an obvious influence on the physical adsorption effect of Ca–Mg/B600. The resistant ability of the solution pH of Ca–Mg/B600 was better than that of Ca–Mg/B300 and Ca–Mg/B450.

2.3.2. Influence of coexisting ions

Coexisting ions are an important factors for P adsorption. Fig. 5 illustrates the P adsorption selectivity of Ca–Mg/biochar in biogas fermentation liquid and P synthesis solution. The P adsorption amount in P synthesis solution was better than that in biogas fermentation liquid, indicating that coexisting ions in a biogas fermentation liquid, such as NO_3^- and Cl^-, can decrease the P adsorption amount of Ca–Mg/biochar because of competition or blocking effect (Yao et al., 2013). The decrease amounts of Ca–Mg/B300, Ca–Mg/B450, and Ca–Mg/B600 were 2.3%, 1.8%, and 1.0%, respectively. Single coexisting ions, such as Cl^- (0.01 mol/L), NO_3^- (0.01 mol/L), and HCO_3^- (0.01 mol/L), could decrease 4.3%, 11.7%, and 41.4% of P removal ratio by biochar adsorption, respectively (Yao et al., 2011b). The mixture of competing compounds could reduce about 60% of P adsorbed amount for biochar adsorption (Yao et al., 2013). The results obtained in the present study were better than the results of Yao et al. (2011b, 2013), and demonstrated that the chemical action of MgO and CaO nanoparticles could reduce the negative interaction effects of coexisting ions and enhance P adsorption selectivity. Huang et al. (2014) found that cation loaded materials, such as $La(OH)_3$-modified exfoliated vermiculites, can decrease the negative effects of coexisting ions on P adsorption. The results were similar to the results of the present study. Furthermore, with increasing synthesis temperature of Ca–Mg/biochar, the influence of coexisting ions on P adsorption selectivity decreased. Considering that the physical action of Ca–Mg/biochar adsorption increased with increasing synthesis temperature, the physical action of mesoporous structure could also enhance the resistant of Ca–Mg/biochar to the influence of coexisting ions.

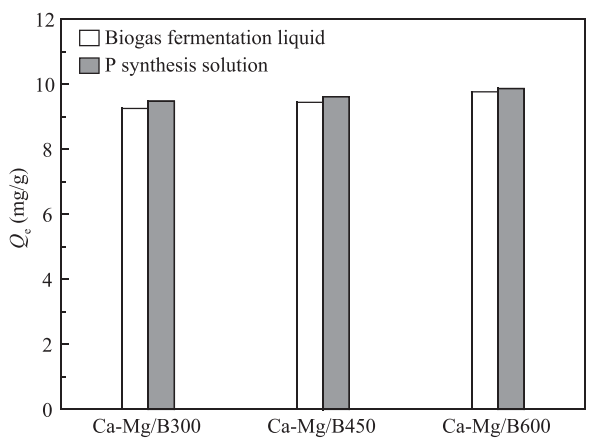

Fig. 5 – Coexisting ion influence on P adsorption selectivity of Ca–Mg/biochar. (Q_e represents the P adsorbed amount at adsorption equilibrium)

2.4. P available of postsorption Ca–Mg/biochar

Continuous extraction and interval extraction experiments were performed to investigate the P available characterization of postsorption Ca–Mg/biochar. The continuous extraction experiment (Fig. 6) shows that the P release rate of postsorption Ca–Mg/biochar was slow. The release rate in DI was slower than that in citric acid DI. According to the adsorption or desorption mechanisms, the stronger the ability of adsorption, the weaker the ability of desorption (Yao et al., 2013). Although Ca–Mg/biochar strongly adsorbed P in an alkalescent solution, the postsorption Ca–Mg/biochar could desorb P quite well in an acid solution. Therefore, the postsorption Ca–Mg/biochar is more suitable as fertilizer for an acid environment. Pseudo second-order kinetic equation was used to describe the P release process of postsorption Ca–Mg/biochar. The formula is expressed as follows:

$$\frac{t}{C_t} = \frac{1}{k_{ds} C_e^{\,2}} + \frac{t}{C_e} \tag{11}$$

where, C_t (mg/L) represents the P concentration at t, C_e (mg/L) represents the P concentration at desorption equilibrium, and k_{ds} (L/(mg·hr)) represents the kinetic constant of second-order equation. The P releasing process of postsorption Ca–Mg/biochar was confirmed by the pseudo second-order kinetic equation with $R^2 > 0.98$. The releasing amounts of postsorption Ca–Mg/biochar in two extraction liquids were in the order of Ca–Mg/B600 > Ca–Mg/B450 > Ca–Mg/B300, a sequence that could be attributed to the total P adsorbed amounts, which were Ca–Mg/B600 > Ca–Mg/B450 > Ca–Mg/B300. In addition, the presence of impregnated CaO and MgO nanoparticles in Ca–Mg/B300, Ca–

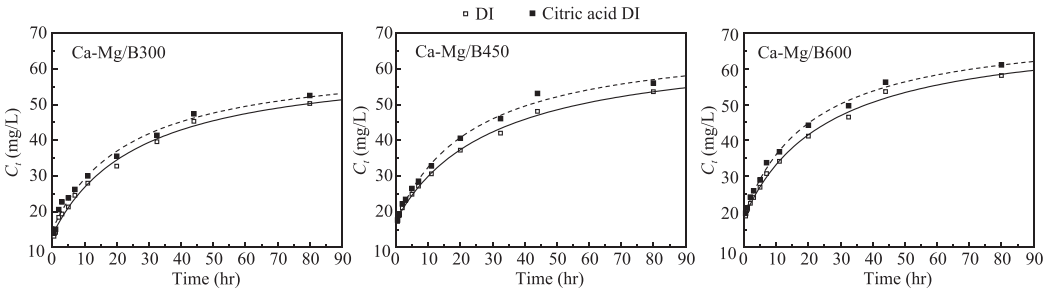

Fig. 6 – Continuous water extraction of postsorption Ca–Mg/biochar. (C_t represents P concentration at time *t*)

Mg/B450, and Ca–Mg/B600 did not have obviously different effects on P release.

Given the intense interaction between Ca, Mg and P, only a small amount of P was released when the extraction liquid reached equilibrium. However, results of the interval extraction experiment (Fig. 7) showed that P can be persistently released from postsorption Ca–Mg/biochar with an interval replacement of fresh extraction liquid. Ca–Mg/B300, Ca–Mg/B450, and Ca–Mg/B600 could release 1.43%, 1.58%, and 1.66% of total adsorbed P per interval time in DI, and 1.53%, 1.68%, 1.77% of total adsorbed P per interval time in citric acid DI. The postsorption Ca–Mg/biochar could persistently release P, and the released P could be used as a slow-release fertilizer. Huang et al. (2014) used $La(OH)_3$-modified exfoliated vermiculites to achieve high P adsorption capacity, but the P desorption clearly decrease per interval time. Pitakteeratham et al. (2013) desorbed P from zirconium sulfate-surfactant micelle, but did not obtain regular and stable desorption. The findings of the present study demonstrated that the P available character of postsorption Ca–Mg/biochar is better than that of other cation modified functional materials. The real application of postsorption Ca–Mg/biochar in soil for plant growth will be performed in further research.

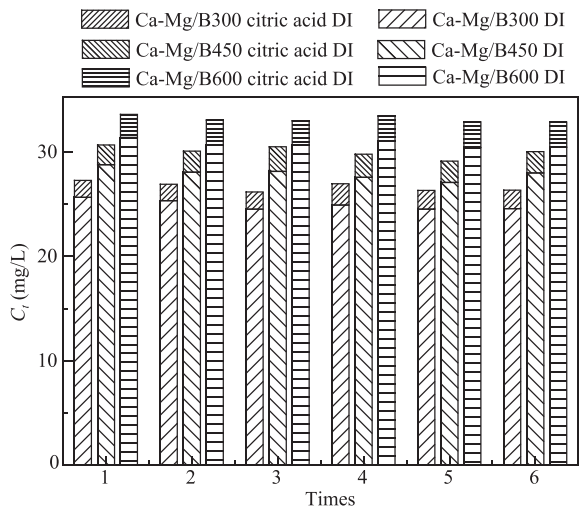

Fig. 7 – Interval water extraction of postsorption Ca–Mg/biochar. (C_t represents P concentration at time *t*)

3. Conclusions

The synthesized Ca–Mg/biochar was rich in the organic functional groups of hydroxyl, carboxyl, carbonyl, and methoxyl, as well as the nanoparticles of CaO and MgO. With increasing synthesis temperature, the yield decreased, BET surface area increased, C content increased, H content decreased, and N content remained basically the same. The P adsorption of Ca–Mg/biochar could be accelerated by nano-CaO and nano-MgO particles and reached adsorption equilibrium after 360 min. It was endothermic, spontaneous, and showed an increase in disorder of the solid–liquid interface. Furthermore, it could be fitted by the Freundlich model. The maximum P adsorption amounts were 294.22, 315.33, and 326.63 mg/g. The P adsorption selectivity of Ca–Mg/biochar could not be significantly influenced by the typical pH level of biogas fermentation liquid. The nano-CaO and nano-MgO particles could reduce the negative interaction effects of coexisting ions in biogas fermentation liquid. The P releasing amounts of postsorption Ca–Mg/biochar were in the order of Ca–Mg/B600 > Ca–Mg/B450 > Ca–Mg/B300. The postsorption Ca–Mg/biochar could persistently release P and is more suitable for an acid environment.

Acknowledgments

The authors are indebted to Prof. Paul Westerhoff in Arizona State University for his insightful comments and suggestions that significantly improved the manuscript. The work was supported by the Specialized Research Fund for the Doctoral Program of Higher Education of China (No. 20120008120013), the National Natural Science Foundation of China (No. 31401944), the Beijing Natural Science Foundation (No. 6144026), the China Scholarship Council (No. 201206355006), and the Chinese Universities Scientific Fund of China Agricultural University (No. 2011JS169). The Analytical Instrumentation Center of Peking University is also being thanked.

REFERENCES

Al-Wabel, M.I., Al-Omran, A., El-Naggar, A.H., Nadeem, M., Usman, A.R., 2013. Pyrolysis temperature induced changes in characteristics and chemical composition of biochar produced from conocarpus wastes. Bioresour. Technol. 131, 374–379.

APHA (American Public Health Association), 2012. Standard Methods for the Examination of Water and Wastewater (Washington DC, USA).
Chen, Y.C., Lu, C., 2014. Kinetics, thermodynamics and regeneration of molybdenum adsorption in aqueous solutions with NaOCl-oxidized multiwalled carbon nanotubes. J. Ind. Eng. Chem. 20 (4), 2521-2517.
Chen, J., Kong, H., Wu, D., Chen, X., Zhang, D., Sun, Z., 2007. Phosphate immobilization from aqueous solution by fly ashes in relation to their composition. J. Hazard. Mater. 139 (2), 293–300.
Chen, B., Zhou, D., Zhu, L., 2008. Transitional adsorption and partition of nonpolar and polar aromatic contaminants by biochars of pine needles with different pyrolytic temperatures. Environ. Sci. Technol. 42 (14), 5137–5143.
Chen, B., Chen, Z., Lü, S., 2011. A novel magnetic biochar efficiently sorbs organic pollutants and phosphate. Bioresour. Technol. 102 (2), 716–723.
Demirbas, A., 2004. Effects of temperature and particle size on bio-char yield from pyrolysis of agricultural residues. J. Anal. Appl. Pyrolysis 72 (2), 243–248.
Elser, J., Bennett, E., 2011. A broken biogeochemical cycle. Nature 478 (7367), 29–31.
Gaskin, J., Steiner, C., Harris, K., Das, K., Bibens, B., 2008. Effect of low-temperature pyrolysis conditions on biochar for agricultural use. Trans. ASABE 51 (6), 2061–2069.
Geng, W., Nakajima, T., Takanashi, H., Ohki, A., 2009. Analysis of carboxyl group in coal and coal aromaticity by Fourier transform infrared (FT-IR) spectrometry. Fuel 88 (1), 139–144.
Gilbert, N., 2009. Environment: the disappearing nutrient. Nature 461 (7265), 716–718.
Hale, S.E., Alling, V., Martinsen, V., Mulder, J., Breedveld, G.D., Cornelissen, G., 2013. The sorption and desorption of phosphate-P, ammonium-N and nitrate-N in cacao shell and corn cob biochars. Chemosphere 91 (11), 1612–1619.
Hossain, M.K., Strezov, V., Chan, K.Y., Ziolkowski, A., Nelson, P.F., 2011. Influence of pyrolysis temperature on production and nutrient properties of wastewater sludge biochar. J. Environ. Manag. 92 (1), 223–228.
Huang, W.Y., Li, D., Liu, Z.Q., Tao, Q., Zhu, Y., Yang, J., et al., 2014. Kinetics, isotherm, thermodynamic, and adsorption mechanism studies of $La(OH)_3$-modified exfoliated vermiculites as highly efficient phosphate adsorbents. Chem. Eng. J. 236, 191–201.
Johan, E., Shukla, E.A., Matsue, N., Henmi, T., 2013. Fe-treated artificial zeolite as an adsorbent for anionic and cationic pollutants. Procedia Environ. Sci. 17, 285–290.
Loria, E.R., Sawyer, J.E., Barker, D.W., Lundvall, J.P., Lorimor, J.C., 2007. Use of anaerobically digested swine manure as a nitrogen source in corn production. Agron. J. 99 (4), 1119–1129.
Novak, J.M., Lima, I., Xing, B., Gaskin, J.W., Steiner, C., Das, K.C., et al., 2009. Characterization of designer biochar produced at different temperatures and their effects on a loamy sand. Ann. Environ. Sci. 3, 195–206.
Oztürk, N., Bektaş, T.E., 2004. Nitrate removal from aqueous solution by adsorption onto various materials. J. Hazard. Mater. 112 (1), 155–162.
Pitakteeratham, N., Hafuka, A., Satoh, H., Watanabe, Y., 2013. High efficiency removal of phosphate from water by zirconium sulfate-surfactant micelle mesostructure immobilized on polymer matrix. Water Res. 47 (11), 3583–3590.
Rittmann, B.E., Mayer, B., Westerhoff, P., Edwards, M., 2011. Capturing the lost phosphorus. Chemosphere 84 (6), 846–853.
Strezov, V., Popovic, E., Filkoski, R.V., Shah, P., Evans, T., 2012. Assessment of the thermal processing behavior of tobacco waste. Energy Fuels. 26 (9), 5930–5935.
Tang, J., Zhu, W., Kookana, R., Katayama, A., 2013. Characteristics of biochar and its application in remediation of contaminated soil. J. Biosci. Bioeng. 116 (6), 653–659.
Tseng, R.L., Wu, F.C., 2008. Inferring the favorable adsorption level and the concurrent multi-stage process with the Freundlich constant. J. Hazard. Mater. 155 (1–2), 277–287.
Tu, Y.J., You, C.F., 2014. Phosphorus adsorption onto green synthesized nano-bimetal ferrites: equilibrium, kinetic and thermodynamic investigation. Chem. Eng. J. 251, 285–292.
Unlu, N., Ersoz, M., 2006. Adsorption characteristics of heavy metal ions onto a low cost biopolymeric sorbent from aqueous solutions. J. Hazard. Mater. 136 (2), 272–280.
Venkata Mohan, S., Chandrasekhar Rao, N., Karthikeyan, J., 2002. Adsorptive removal of direct azo dye from aqueous phase onto coal based sorbents: a kinetic and mechanistic study. J. Hazard. Mater. 90 (2), 189–204.
Wajima, T., Rakovan, J.F., 2013. Removal behavior of phosphate from aqueous solution by calcined paper sludge. Colloids Surf. A Physicochem. Eng. Asp. 435, 132–138.
Yao, Y., Gao, B., Inyang, M., Zimmerman, A.R., Cao, X., Pullammanappallil, P., et al., 2011a. Biochar derived from anaerobically digested sugar beet tailings: characterization and phosphate removal potential. Bioresour. Technol. 102 (10), 6273–6278.
Yao, Y., Gao, B., Inyang, M., Zimmerman, A.R., Cao, X., Pullammanappallil, P., et al., 2011b. Removal of phosphate from aqueous solution by biochar derived from anaerobically digested sugar beet tailings. J. Hazard. Mater. 190 (1–3), 501–507.
Yao, Y., Gao, B., Chen, J., Yang, L., 2013. Engineered biochar reclaiming phosphate from aqueous solutions: mechanisms and potential application as a slow-release fertilizer. Environ. Sci. Technol. 47, 8700–8708.
Yoon, S.Y., Lee, C.G., Park, J.A., Kim, J.H., Kim, S.B., Lee, S.H., et al., 2014. Kinetic, equilibrium and thermodynamic studies for phosphate adsorption to magnetic iron oxide nanoparticles. Chem. Eng. J. 236, 341–347.
Zhang, M., Gao, B., Yao, Y., Inyang, M., 2013. Phosphate removal ability of biochar/MgAl-LDH ultra-fine composites prepared by liquid-phase deposition. Chemosphere 92 (8), 1042–1047.
Zhang, T., Li, P., Fang, C., Jiang, R.F., 2014. Phosphate recovery from animal manure wastewater by struvite crystallization and CO_2 degasification reactor. Ecol. Chem. Eng. S. 21 (1), 89–99.

Editorial Board of Journal of Environmental Sciences

JOURNAL OF ENVIRONMENTAL SCIENCES

环境科学学报(英文版)

www.jesc.ac.cn

Aims and scope

Journal of Environmental Sciences is an international academic journal supervised by Research Center for Eco-Environmental Sciences, Chinese Academy of Sciences. The journal publishes original, peer-reviewed innovative research and valuable findings in environmental sciences. The types of articles published are research article, critical review, rapid communications, and special issues.

The scope of the journal embraces the treatment processes for natural groundwater, municipal, agricultural and industrial water and wastewaters; physical and chemical methods for limitation of pollutants emission into the atmospheric environment; chemical and biological and phytoremediation of contaminated soil; fate and transport of pollutants in environments; toxicological effects of terrorist chemical release on the natural environment and human health; development of environmental catalysts and materials.

For subscription to electronic edition

Elsevier is responsible for subscription of the journal. Please subscribe to the journal via http://www.elsevier.com/locate/jes.

For subscription to print edition

China: Please contact the customer service, Science Press, 16 Donghuangchenggen North Street, Beijing 100717, China. Tel: +86-10-64017032; E-mail: journal@mail.sciencep.com, or the local post office throughout China (domestic postcode: 2-580).

Outside China: Please order the journal from the Elsevier Customer Service Department at the Regional Sales Office nearest you.

Submission declaration

Submission of the work described has not been published previously (except in the form of an abstract or as part of a published lecture or academic thesis), that it is not under consideration for publication elsewhere. The publication should be approved by all authors and tacitly or explicitly by the responsible authorities where the work was carried out. If the manuscript accepted, it will not be published elsewhere in the same form, in English or in any other language, including electronically without the written consent of the copyright-holder.

Editorial

Authors should submit manuscript online at http://www.jesc.ac.cn. In case of queries, please contact editorial office, Tel: +86-10-62920553, E-mail: jesc@rcees.ac.cn. Instruction to authors is available at http://www.jesc.ac.cn.

Journal of Environmental Sciences (Established in 1989)
Volume 29 2015

Supervised by	Chinese Academy of Sciences	**Published by**	Science Press, Beijing, China
Sponsored by	Research Center for Eco-Environmental		Elsevier Limited, The Netherlands
	Sciences, Chinese Academy of Sciences	**Distributed by**	
Edited by	Editorial Office of Journal of	Domestic	Science Press, 16 Donghuangchenggen
	Environmental Sciences		North Street, Beijing 100717, China
	P. O. Box 2871, Beijing 100085, China		Local Post Offices through China
	Tel: 86-10-62920553; http://www.jesc.ac.cn	Foreign	Elsevier Limited
	E-mail: jesc@rcees.ac.cn		http://www.elsevier.com/locate/jes
Editor-in-chief	X. Chris Le	**Printed by**	Beijing Beilin Printing House, 100083, China

CN 11-2629/X **Domestic postcode: 2-580** **Domestic price per issue RMB ¥ 110.00**

ISSN 1001-0742